*Nanopages 8 (2013), 1–8*
*DOI: 10.1556/Nano.2013.00002*

# Carbon Nanotubes Synthesis over FeCo-Based Catalysts Supported on SBA-16

**D. Carta*[1], S. Bullita[1], A. Falqui[1], M. F. Casula[1], A. Corrias[1] and Z. Kónya[2]**

[1] Dipartimento di Scienze Chimiche e Geologiche and INSTM,
Università di Cagliari, S.S. 554 bivio per Sestu, I-09042 Monserrato, Cagliari, Italy
[2] Department of Applied and Environmental Chemistry, University of Szeged,
Rerrich Bela tér 1, H-6720, Szeged, Hungary

**Abstract.** A series of Fe/Co based nanocomposites where the matrix is mesoporous ordered cubic *Im3m* silica (SBA-16 type) characterized by a three dimensional cage-like structure of pores were obtained by two different approaches: impregnation and gelation. X-ray diffraction and transmission electron microscopy analysis show that after metal loading, calcination at 500 °C and reduction in $H_2$ flux at 800 °C the nanocomposites retain the well-ordered structure of the matrix with cubic symmetry of pores. All nanocomposites prepared were tested for the production of carbon nanotubes by catalytic chemical vapour deposition. Transmission electron microscopy points out that good quality multi-walled carbon nanotubes are obtained.

**Keywords:** mesoporous materials, SBA-16, carbon nanotubes

## 1. Introduction

Metal nanoparticles dispersed in a highly porous support are widely studied for their important biomedical, magnetic and catalytic applications [1]. In fact, the peculiar properties of nanoparticles are due to their small particle size, high surface to volume ratio, morphology and surface coating and their dispersion in a highly porous support preserves these properties, by avoiding their agglomeration and coalescence. In particular, the dispersion of nanoparticles in a porous matrix is of particular interest in catalysis: the matrix not only acts as a support material but also plays an active role in the catalytic process; in fact, the porosity of the matrix influences the accessibility of the active catalytic particles, affecting selectivity and activity. Ordered mesoporous silicas with uniform pore sizes between 20 and 500 Å have attracted much interest as a support for catalytic nanoparticles because of their regularly arranged pore structure and high specific surface area. In particular, nanoparticles of transition metals and their bimetallic alloys supported on ordered mesoporous silica have great potential as catalysts for carbon nanotubes (CNTs) production. The pore sizes in mesoporous silica are in the range of the usual diameters of CNTs and the uniform distribution of pore dimensions where nanoparticles are allocated facilitates the production of CNTs with a narrow distribution of diameters. In particular, a cubic mesoporous silica support, such as SBA-16, characterized by a three-dimensional (3D) ordered cage-like network of interconnected pores (*Im3m* structure), large cell parameter and thick walls, appears to be the most promising support for catalytic applications, providing an easy accessibility and diffusion of reactants in all directions and being highly thermally stable. Unlike the hexagonal SBA-15 form of mesoporous silica, where the pores form parallel channels that can be accessible in only one direction, the cubic mesoporous silica has not been studied extensively, probably because it can only be produced in a narrow range of conditions [2]. In particular,

* Corresponding author. E-mail: cartadany@hotmail.com

very little work has been done on the synthesis of FeCo nanoparticles dispersed in a cubic mesoporous matrix [3]. Films of nanocomposites of Fe nanoparticles dispersed in SBA-16 have been prepared and used as catalyst for the growth of aligned CNTs [4, 5] and Fe-filled CNTs [6]. However, it has been shown that FeCo alloy nanoparticles are more effective than the isolated Fe and Co nanoparticles for the growth of CNTs [7].

We have recently succeeded in preparing a series of catalysts containing nanoparticles of FeCo alloy dispersed in ordered 3D cubic SBA-16 type matrix using a one-step, templated-assisted sol-gel technique [8, 9] and by impregnation on SBA-16 [10, 11] prepared synthesized by the original method developed by the Stucky group [12]. We have successfully tested the nanocomposites prepared by one-step technique for carbon nanotubes (CNTs) production by catalytic chemical vapour deposition (CCVD) [8, 9].

In this work, we show the results of the catalytic tests for the production of CNTs carried out using nanocomposites prepared by two different approaches: gelation [3] and impregnation on a SBA-16 type matrix prepared according to an improved synthetic method, which makes use of butanol as a co-surfactant [13, 14].

## 2. Experimental

### *2.1. Nanocomposites prepared by gelation*

The synthesis of the nanocomposites prepared by gelation was adapted by a previously developed sol-gel route reported in reference 3. Two different nanocomposites were prepared: one containing only Co and one containing Fe and Co (Fe:Co ratio 1:1) dispersed in the SBA-16 type matrix. In both cases a solution was prepared by mixing 8 g of TEOS (Aldrich 98%), 5 g of EtOH (99.8%) and 0.71 g of HCl 0.77 M. This solution was stirred for 45 minutes, then it was added to a solution containing 24 g of EtOH, 2.6 g of Pluronic F127 (P127, Aldrich) and 3 g of a HCl 0.07 M and stirred for 20 hours at 25 °C. To this solution 0.60 g of $Co(NO_3)_2 \cdot 6H_2O$ (Aldrich, 98%) corresponding to a nominal ratio of 5 wt % Co/(Co $+SiO_2$) were added, in order to obtain the sample with only Co. The nanocomposite containing Fe and Co was prepared by adding 0.428 g of $Fe(NO_3)_3 \cdot 9H_2O$ (Aldrich, 98%) and 0.308 g of $Co(NO_3)_2 \cdot 6H_2O$ (Aldrich, 98%) corresponding to a nominal ratio of 5 wt % FeCo/(FeCo $+SiO_2$). The obtained solutions were then transferred to a teflon container (10 cm diameter, 5 cm height) covered with pierced parafilm and left at room temperature until gelation. Gels were then calcined in air with a heating step of 1 °C/min up to 500 °C and hold at 500 °C for 6 hours. Finally, a reduction treatment in $H_2$ flux was performed for each nanocomposite, with a heating step of 10°C/min up to 800 °C and hold at 800 °C for 2 hours to promote the formation of metallic nanoparticles. The nanocomposite containing only Co, and the one containing Fe and Co after calcination at 500 °C will be hereafter indicated as G_Co_500 and G_Fe1Co1_500, while the corresponding reduced samples will be hereafter indicated as G_Co_r800 and G_Fe1Co1_r800.

### *2.2. Nanocomposites prepared by impregnation*

A 0.3 g of SBA-16 prepared according to the synthetic method described by Kleitz et al. [15]. were impregnated with 10 mL of an aqueous solution of $Fe(NO_3)_3 \cdot 9H_2O$ (Aldrich, 98%) and $Co(NO_3)_2 \cdot 6H_2O$ (Aldrich, 98%), with a total metal molar concentrations of Fe and Co ions of 0.4 M and a Fe:Co ratio of 1:1 and vigorously stirred for 24 hours. The impregnated support was separated from the solution by centrifugation. The sample was then calcined in

*Table 1.* List of prepared nanocomposites

| Acronym | Thermal treatment |
|---|---|
| G_Co_500 | Calcined in air at 500 °C |
| G_Co_r800 | Reduced in $H_2$ at 800 °C |
| G_Fe1Co1_500 | Calcined in air at 500 °C |
| G_Fe1Co1_r800 | Reduced in $H_2$ at 800 °C |
| I_Fe1Co1_500 | Calcined in air at 500 °C |

air with a heating step of 1°C/min up to 500 °C and hold at 500 °C for 6 hours, and will be thereafter indicated as I_Fe1Co1_500.

A list of the samples studied is reported in *Table 1.*

### *2.3. Synthesis of CNTs*

CNTs were grown by CCVD of acetylene ($C_2H_2$) at 750 °C over all prepared catalysts. One hundred mg of catalyst were placed in a quartz plate which was inserted into a reactor under a flow of 300 mL/min $N_2$ for 10 minutes. Then, the reactor was inserted into a furnace at 750 °C and $N_2$ was replaced with $C_2H_2$ (30 mL/min) which was fluxed for 20 minutes.

### *2.4. Characterisation*

X-ray diffraction patterns were recorded using Cu Kα radiation on a Panalytical Empyrean diffractometer equipped with a X'Celerator linear detector. Data were collected in Bragg–Brentano geometry with a graphite monochromator on the diffracted beam. The scans were collected within the range of 15°–85° (2θ).

Conventional Transmission Electron Microscopy (TEM) images were recorded either on a JEOL 200CX microscope operating at 200 kV or on a Jeol TEM 1011 Microscope, operating at 125 kV, both equipped with a W thermionic electron source.

High Resolution Transmission Electron Microscopy (HRTEM) images were recorded on a Jeol 2100F microscope, equipped with a Schottky field emission gun operating at 200 kV.

## 3. Results and discussion

*Figures 1A* and *1D* show the wide-angle X-ray Diffraction (XRD) patterns of the nanocomposites prepared by gelation, after calcination at 500 °C and after reduction at 800 °C, respectively. A halo arising from the amorphous silica matrix is observed in all the nanocomposites at 2θ ~ 20–30°. The pattern of G_Co_500 presents two broad peaks at 2θ ~ 35° at 2θ ~ 60° that correspond to the structure of a layered phyllosilicate, the cobalt silicate hydroxide $Co_3Si_2O_5(OH)_4$ (PDF Card n. 21-0872) while the pattern of G_Fe1Co1_500 does not show any Bragg peaks indicating that Fe and Co are present in form of intermediate phases which are highly disordered and/or dispersed. The pattern of the G_Co_r800 reduced sample, shows three peaks at 2θ ~ 44°, 51° and 75° ascribed to the *fcc* Co phase (PDF Card n. 15-806), indicating that upon reduction, the cobalt silicate hydroxide phase is reduced to pure fcc Co nanoparticles. G_Fe1Co1_r800 shows the three peaks ascribed to the *fcc* Co phase (PDF

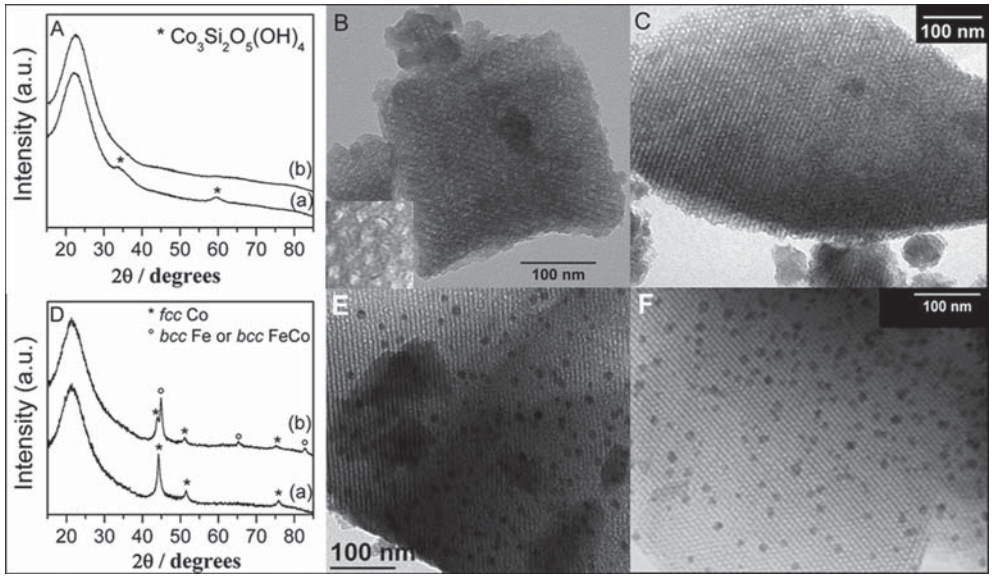


*Figure 1.* (A) XRD patterns of (a) G_Co_500; (b) G_Fe1Co1_500; (B) TEM image of G_Co_500; (C) TEM image of G_Fe1Co1_500; (D) XRD patterns of (a) G_Co_r800; (b) G_Fe1Co1_r800; (E) TEM image of G_Co_r800; (F) TEM image of G_Fe1Co1_r800

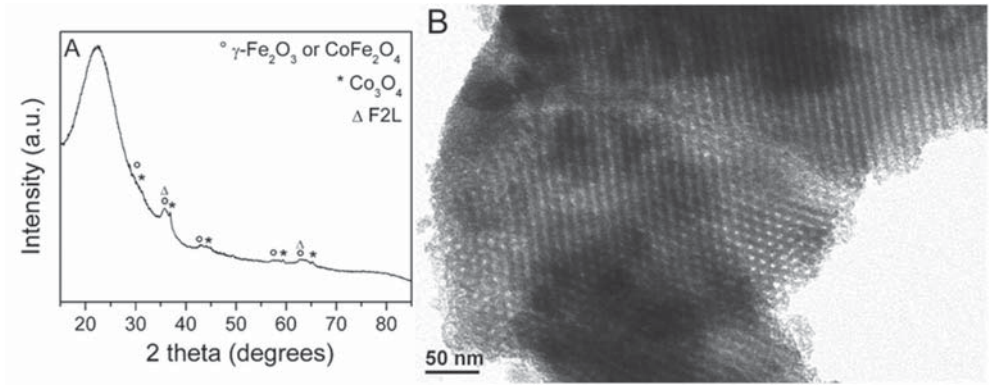


*Figure 2.*Wide angle XRD (A) and TEM image (B) of I_Fe1Co1_500

Card n. 15-806) and three additional peaks at 2θ ~ 45°, 65° and 83° that could be due to pure *bcc* α-Fe (PDF Card n. 6-696) or to the *bcc* FeCo alloy (PDF Card n. 44-1433). It has to be noted that XRD is not conclusive for the identification of all the phases present in the samples containing both Fe and Co phases. However, extended X-ray absorption fine structure (EXAFS) and X-ray absorption near-edge structure (XANES) results (not shown here) have confirmed that after reduction at 800 °C, *bcc* Fe and *fcc* Co are present as two separated phases in G_Fe1Co1_r800.

*Figures 1B/C* show the TEM images of the nanocomposites prepared by gelation after calcination at 500 °C and *Figures 1E/F* show the TEM images of same nanocomposites after reduction at 800 °C. A highly ordered arrangement of mesopores which is consistent

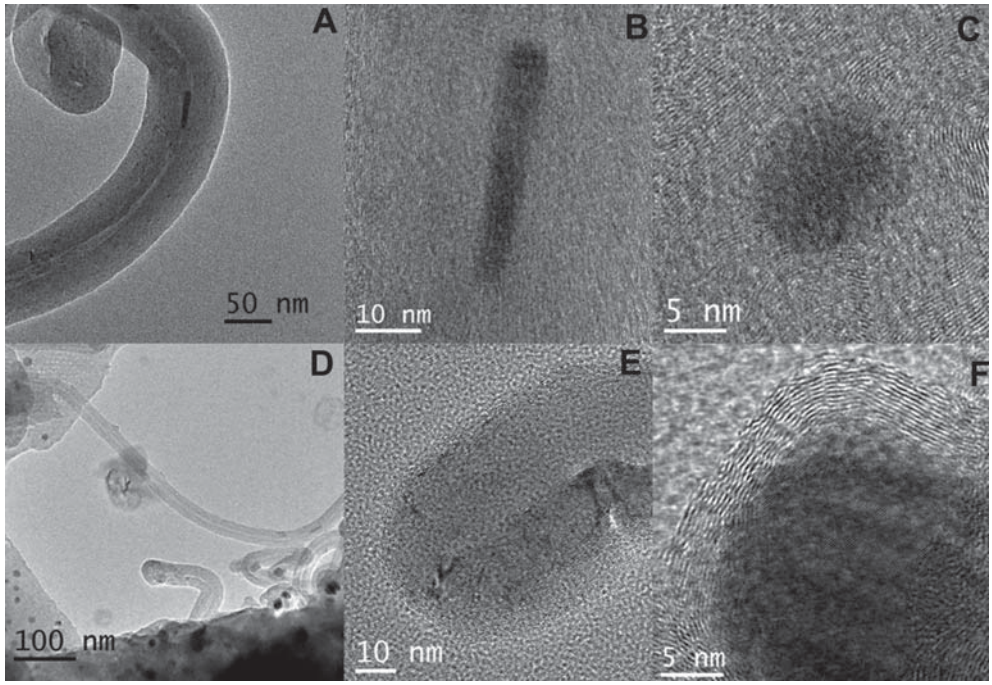


*Figure 3.* HRTEM images of: G_Co_500_CNT (A, B, C) and G_Co_r800_CNT (D, E, F)

with a cubic mesostructure can be observed in all samples. The TEM image of G_Co_500 *(Fig. 1B)* gives clear evidence of the cobalt silicate hydroxide in the form of one-dimensional shape nanoneedles (acicular nanoparticles) homogeneously dispersed in the regular arrays of mesopores of the silica structure. Similar images were observed in Fe/Co containing aerogel silica matrix [16]. Upon reduction, spherical nanoparticles (8–12 nm) are formed within the SBA-16 type matrix, as clearly shown by the TEM images of G_Co_800 and G_Fe1Co1_r800, reported in *Figs 1E* and *1F,* respectively. The ordered porous structure is clearly preserved after reduction at 800 °C.

The XRD pattern of the calcined sample prepared by impregnation, shown in *Fig. 2A,* shows weak peaks which can be ascribed to $Co_3O_4$ and to an additional phase which could be either 2-line ferrihydrite (F2L), a very poorly crystalline Fe(III) oxyhydroxide [17], γ-$Fe_2O_3$ (PDF-2 Card n. 39-1346) or $CoFe_2O_4$ (PDF-2 Card n. 22-1086). As observed for G_Fe1Co1_r800, XRD analysis is not conclusive. As reported in ref. 11, EXAFS and XANES analysis have shown that two separated phases are present in I_Fe1Co1_500: $Co_3O_4$ and F2L. The TEM image reported in *Fig. 2B* confirms that the structural ordering and cubic symmetry of the support is maintained after metal loading and calcination, as observed for the nanocomposites prepared by gelation.

Due to the textural and microstructural features of the obtained nanocomposites, the potential of these materials in gas phase catalysis was tested. In particular, all samples were used as catalysts for CNTs production. It is well known that metal or alloy nanoparticles act as active sites for the production of CNTs. However, it has been reported that better catalytic performances are obtained if the metals/alloys are generated *in situ* during the CNT production from the hydrogen formed during the reaction [18, 19]. In this case we tested both the calcined samples G_Co_500, G_Fe1Co1_500 and I_Fe1Co1_500 were active

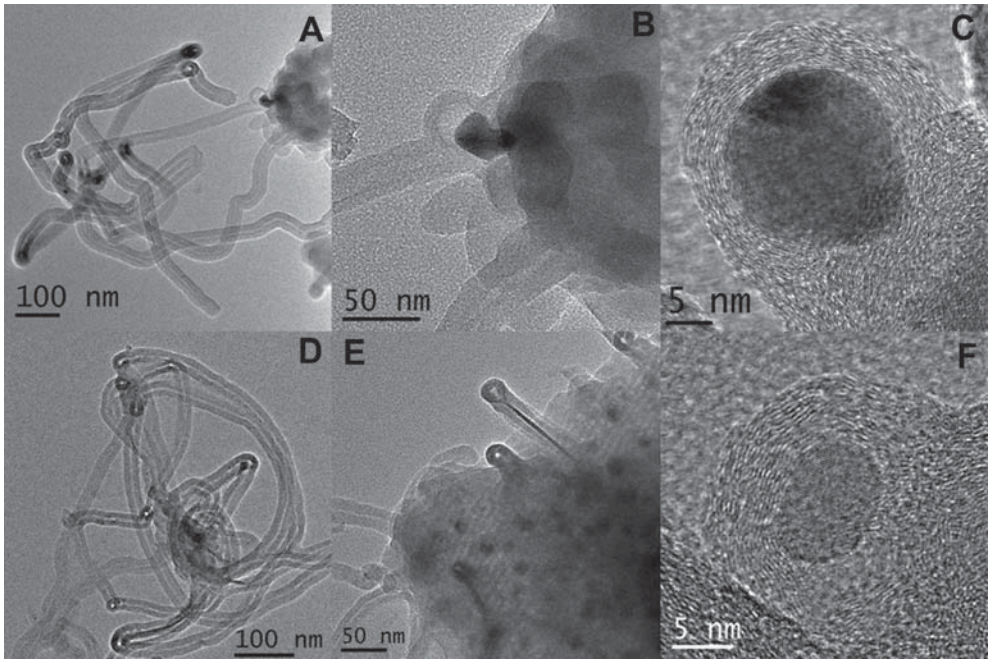


*Figure 4.* HRTEM images of: G_Fe1Co1_500_CNT (A, B, C) and G_Fe1Co1_r800_CNT (D, E, F)

nanoparticles were obtained by the *in situ* reduction of the oxidized species and the reduced samples G_Co_r800 and G_Fe1Co1_r800 were active nanoparticles were present prior to the CNTs production.

TEM and HRTEM images of G_Co_500 and G_Fe1Co1_500 and those of G_Co_r800 and G_Fe1Co1_r800 after CNTs production, are reported in *Figs 3* and *4,* respectively. All the images give evidence of the formation of multi-walled CNTs (MWCNTs). The produced MWCNTs have an inner diameter in the range 4–6 nm and an outer diameter in the range 20–30 nm with a rough estimation of the average number of walls of 14. Only in G_Co_500 MWCNTs thicker walls were observed. Some images show some either spherical *(Figs 3C, 4C, 4F)* or elongated nanoparticles *(Figs 3A, 3B, 4E)* entrapped inside the MWCNTs. Some other images clearly show single nanoparticles surrounded by graphene layers *(Figs 3C, 3F, 4C, 4F).*

TEM images of I_Fe1Co1_500 after CNTs production, reported in *Fig. 5,* give evidence of the formation of a considerable amount of MWCNTs. In images 5A and 5C, portions of the ordered silica matrix along with the produced MWCNTs can be seen. In image 5B, the presence of some either spherical or ellipsoidal nanoparticles entrapped inside the MWCNTs is evident. It has also to be noted (image 5B) the presence of a curled and helical MWCNT. Nanoparticles both embedded in the matrix and entrapped inside the MWCNTs are clearly visible as bright spots in the dark field image 5D.

It has to be noted that the MWCNTs obtained by using as catalysts the nanocomposites containing Fe and Co phases are of better quality than those obtained by using the sample containing only Co, as expected. In particular, TEM images indicate that the quality of MWCNTs obtained by using I_Fe1Co1_500 are of very high quality. In addition, the images

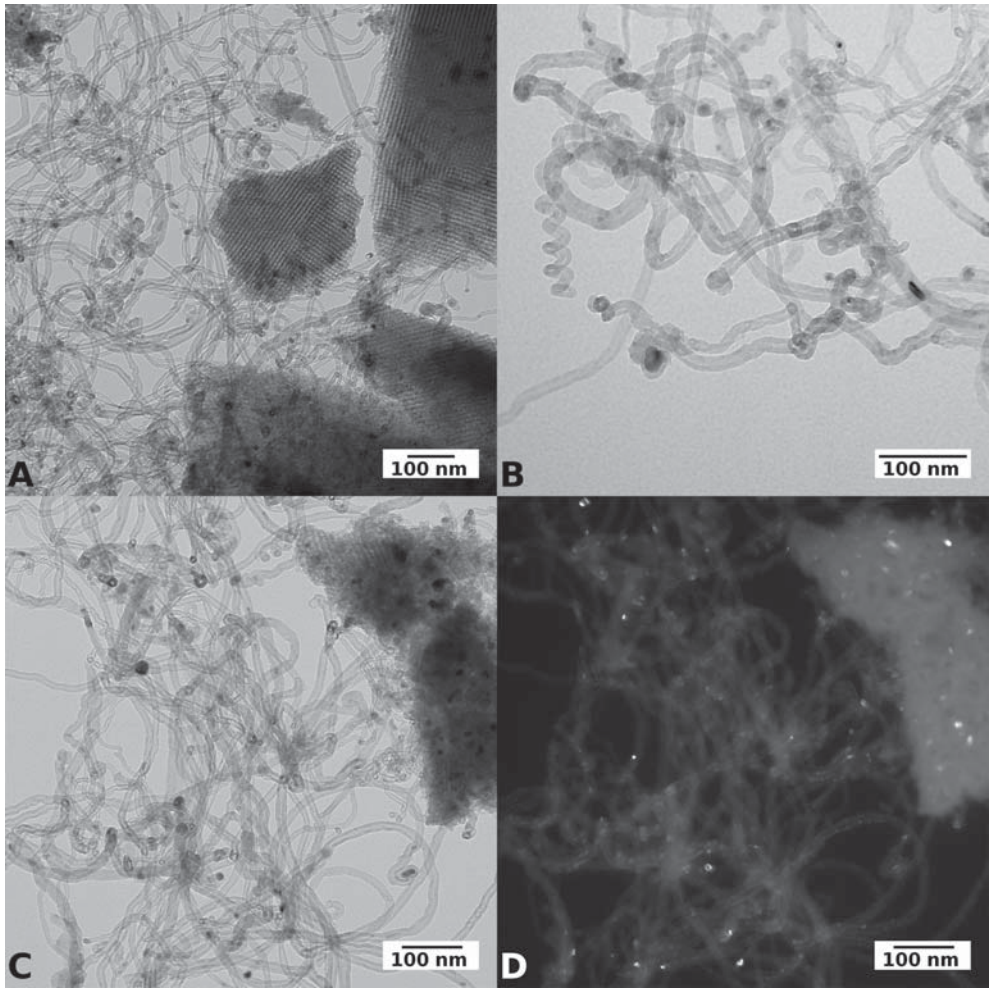


*Figure 5.* TEM images of I_Fe1Co1_500_CNT

suggest an higher yield in MWCNTs production which will be investigated by quantitative routes. The preliminary results obtained on MWCNTs production are very promising suggesting that films of FeCo-SBA-16 could be used to fabricate ordered CNTs patterns with aligned orientation.

## 4. Conclusions

Nanocomposites based on Fe/Co nanophases dispersed in a highly ordered cubic mesoporous silica matrix SBA-16 were prepared using either a gelation or an impregnation technique followed by post-synthesis heating treatments including reduction in $H_2$ at 800 °C. TEM confirmed that the ordered cubic mesoporous structure is preserved after metal loading and post-synthesis reactive thermal treatments. It has been shown that metal or alloy nanoparticles act as active sites for the production of CNTs.

## 5. Acknowledgements

This work has been carried out within the framework of the project “NANOCAT” funded through the SEED call of the Italian Institute of Technology (IIT) and with the contribution of “Ministero degli Affari Esteri, Direzione Generale per la Promozione del Sistema Paese”.

## References

[1] R. J. White, R. Luque, V. L. Budarin, J. H. Clark, D. J. Macquarrie, *Chem. Soc. Rev.,* **38,** 481, (2009).
[2] D. Zhao, Q. Huo, J. Feng, B. F. Chmelka, G. D. Stucky, *J. Am. Chem. Soc.*, **120,** 6024, (1998).
[3] S. Costacurta, L. Malfatti, P. Innocenzi, H. Amenitsch, A. Masili, A. Corrias, M. F. Casula, *Micropor. Mesopor. Mat.,* **115,** 338, (2008).
[4] G. Zheng, H. Zhu, Q. Luo, Y. Zhou, D. Zhao, *Chem. Mater.,* **13,** 2240, (2001).
[5] L. Huang, S. J. Wind, S. P. O’Brien, *Nano Lett.,* **3,** (3) 299, (2003).
[6] K. Shi, Y. Chi, H. Yu, B. Xin, H. Fu, *J. Phys. Chem. B.,* **109,** 2546, (2005).
[7] J. Zhu, M. Yudasaka, S. Iijima, *Chem. Phys. Lett.,* **380,** 496, (2003).
[8] D. Carta, M. F. Casula, A. Corrias, A. Falqui, Á. Dombovári, A. Gálos, Z. Kónya, *J. Nanosci. Nanotechno.,* **11,** 1, (2011).
[9] D. Carta, G. Navarra, A. Falqui, Z. Kónya, A. Corrias, *RSC Advances,* **2,** 7886, (2012).
[10] D. Carta, M. F. Casula, S. Bullita, A. Falqui, A. Corrias *J. Nanopart. Res.,* **13,** 3489, (2011).
[11] D. Carta, G. Mountjoy, R. Apps, A. Corrias, *J. Phys. Chem. C,* **116,** 12353 (2012).
[12] D. Zhao, Q. Huo, J. Feng, B. F. Chmelka, G. D. Stucky, *J. Am. Chem. Soc.,* **120,** 6024, (1998).
[13] F. Kleitz, L. A. Solovyov, G. M. Anilkumar, S. H. R. Choi, Ryoo, *Chem. Comm.,* **13,** 1536, (2004).
[14] F. Kleitz, T. Czuryszkiewicz, L. A. Solovyov, M. Lindén, *Chem. Mater.,* **18,** 5070, (2006).
[15] F. Kleitz, T-W Kim, R. Ryoo, *Langmuir,* **22,** 440, (2006).
[16] D. Carta, M. F. Casula, A. Corrias, A. Falqui, D. Loche, G. Mountjoy, W. Peng, *Chem. Mater.,* **21,** 945, (2009).
[17] J. Zhao, F. E. Huggins, Z. Feng, G. P. Huffman, *Clay Clay Miner.* **42,** 737, (1994).
[18] P. Ramesh, T. Okazaki, R. Taniguchi, J. Kimura, T. Sugai, K. Sato, Y. Ozeki, H. Shinohara, *J. Phys. Chem. B,* **109,** 1141, (2005).
[19] Y. Yang, Z. Hu, Y. N. Lu, Y. Chen, *Mater. Chem. Phys.,* **82,** 440 (2003).